Bull. Mater. Sci., Vol. 40, No. 7, December 2017, pp. 1421–1428
https://doi.org/10.1007/s12034-017-1502-1

Role of reactive species in the photocatalytic degradation of amaranth by highly active N-doped WO_3

HANGGARA SUDRAJAT and SANDHYA BABEL*
School of Biochemical Engineering and Technology, Sirindhorn International Institute of Technology, Thammasat University, Pathum Thani 12121, Thailand
*Author for correspondence (sandhya@siit.tu.ac.th)

MS received 27 July 2016; accepted 7 April 2017; published online 6 December 2017

Abstract. A novel, highly visible light active N-doped WO_3 (N-WO_3) is successfully synthesized via thermal decomposition of peroxotungstic acid–urea complex. The photocatalytic activity of N-WO_3 is evaluated for the degradation of amaranth (AM) dye under visible and UVA light along with the role of reactive species, which has not yet been studied for N-WO_3 photocatalysts. Doping of N into substitutional and interstitial sites of WO_3 is confirmed by X-ray photoelectron spectroscopy and X-ray absorption near-edge spectroscopy. At a pH of 7, 1 g l^{-1} of N-WO_3 can completely degrade 10 mg l^{-1} of AM within 1 h under visible and UVA light. For the degradation of AM by N-WO_3 under visible and UVA light, h^+ is found to be the main reactive species, while $^{\bullet}OH$ contributes to a lesser extent. On the contrary, $^1O_2$, $^{\bullet}O_2^-$ and e^- show negligible roles. The crucial role of h^+ indicates effective suppression of electron–hole recombination after N doping. Dye sensitization and oxidation by reactive species are found to be the major pathway for the degradation of AM under visible and UVA light, respectively.

Keywords. Nitrogen doping; photocatalysis; visible light active; reactive species; amaranth.

1. Introduction

Over the past decade, advanced oxidation processes (AOPs), which are capable of generating various reactive radicals, have been proposed for the degradation of toxic and/or recalcitrant compounds in wastewaters. Among AOPs, semiconductor photocatalysis have received great attention due to its clean and solar-driven process, versatility and low-cost of operation at mild conditions.

Of a variety of semiconductors, tungsten oxide (WO_3) seems suitable as it posseses narrow band gap, very deep valence band (VB) potential and high stability [1–3]. However, despite its ability to effectively absorb visible light, pristine WO_3 shows poor visible light activity. This is because its conduction band (CB) potential is very low [4–9]. Thus, the photogenerated electrons, accumulated in the CB cannot be consumed by electron acceptors, resulting in fast recombination with the holes in the VB. It is seen that visible light absorption of WO_3 does not necessarily lead to visible light activity.

To increase the visible light response and the visible light activity of WO_3, N doping appears to be a promising strategy. N can introduce a new energy level within the band gap, thereby extending the spectral response to longer wavelengths and prevents an electron–hole pair from recombination by trapping the electron, thereby increasing photocatalytic activity. Its similar size with O and its lower electronegativity than that of O may also enable homogeneous doping of N within the doped matrix.

The key factor controlling the efficiency of photocatalytic degradation of organic compounds is the type of reactive species generated upon irradiation. However, this aspect has not yet been studied for N-WO_3 photocatalysts. Therefore, in this research, the role of reactive species on the degradation of amaranth (AM), a recalcitrant organic compound, by N-doped WO_3 (N-WO_3) under visible and UVA light is investigated. A mechanism of AM degradation by N-WO_3 is proposed. The effects of operating parameters and inorganic ions are also studied.

2. Materials and methods

2.1 *Materials*

All chemicals were of analytical grade. Tungstic acid (H_2WO_4, Aldrich), hydrogen peroxide solution (H_2O_2, 35 wt%, Aldrich), urea ($CO(NH_2)_2$, Aldrich), AM ($C_{20}H_{11}N_2Na_3O_{10}S_3$, Aldrich), commercial WO_3 (Aldrich), potassium iodide (KI, Aldrich), isopropanol ($(CH_3)_2CHOH$, Aldrich), sodium azide (NaN_3, Aldrich), 2-chloroethanol ($Cl(CH_2)_2OH$, Aldrich), *p*-benzoquinone ($C_6H_4O_2$, Aldrich), sodium chloride (NaCl, Chameleon reagent), sodium nitrate ($NaNO_3$, Aldrich), sodium carbonate (Na_2CO_3, Chameleon

reagent), sodium sulphate (Na_2SO_4, Chameleon reagent), ammonium sulphate ($(NH_4)_2SO_4$, Chameleon reagent) and calcium sulphate ($CaSO_4$, Chameleon reagent) were used as received without further purification. Milli-Q water was used in all the processes.

2.2 *Synthesis*

N-WO_3 was synthesized by thermal decomposition of peroxotungstic acid–urea complex. The peroxotungstic acid was obtained through the reaction of H_2WO_4 with H_2O_2. About 3.75 g of H_2WO_4 was dispersed in 75 ml of water with continuous stirring followed by addition of 25 ml of aqueous H_2O_2 into the dispersion. The reaction mixture was then stirred for 24 h at 40°C. After drying, the obtained powder was dissolved in 75 ml of hot water with continuous stirring for 1 h at 75°C. The solid product was subsequently ground with 1.8 g of $CO(NH_2)_2$ in an agate mortar for 30 min. The ground mixture was calcined at 500°C for 3 h in a muffle furnace to form crystalline N-WO_3 with orange–red colour. The N-WO_3 was washed with water followed by ethanol prior to drying at 100°C for 24 h. Furthermore, pristine N-WO_3 was synthesized by the same method without adding urea. For comparative purposes, N-WO_3 was also synthesized using a similar manner but with commercial WO_3 (c/WO_3) as starting material, which is denoted as c/N-WO_3. About 3.48 g of c/WO_3 was ground with 1.8 g of $CO(NH_2)_2$ in an agate mortar for 30 min followed by calcination, washing and drying.

2.3 *Characterization*

The infrared spectra were recorded by a Fourier transform infrared spectrometer (FT-IR-610, Jasco). The X-ray diffraction (XRD) patterns were collected on a Bruker D8 diffractometer (Cu Kα radiation, $\lambda = 1.5406$ Å). The morphological properties were observed by transmission electron microscopy (JEM 2100, Jeol). The textural properties were examined using N_2 adsorption–desorption isotherms at the liquid nitrogen temperature of 77 K by an adsorption instrument (Belsorp 28SA, Bel). The diffuse reflectance spectra were obtained from a UV-Vis-NIR spectrophotometer (Cary 5000, Agilent) with $BaSO_4$ as reflectance standard. The chemical state of N dopant was verified by X-ray photoelectron spectroscopy (XPS) (Axis Ultra DLD, Kratos Analytical) with Al K α radiation and X-ray absorption near-edge spectroscopy (XANES) at Beamline 3.2a of the Synchrotron Light Research Institute (public organization), Thailand. The zeta potentials were measured as a function of pH using an electrophonic light scattering spectrophotometer (ELS-8000, Otsuka).

2.4 *Photocatalytic activity evaluation*

The photocatalytic activity of the catalyst was evaluated by the degradation of AM under visible and UVA light. A 100 ml of suspension containing known concentrations of the dye and the catalyst was transferred into a batch photoreactor. Dilute NaOH and HCl were used to adjust the suspension pH to a desired level. To attain adsorption–desorption equilibrium, the suspension was magnetically stirred at 200 rpm in the dark for 2 h. A metal halide lamp 160 W (Philips), with an irradiance of 144.7 W m^{-2} and a blacklight lamp 13 W (General Electric) with an irradiance of 3.5 W m^{-2} were used as visible and UVA light sources, respectively. The metal halide lamp was equipped with a cut-off filter, removing radiation below 400 nm. The lamp was switched on to initiate a photocatalytic reaction. After a given irradiation time, the suspension was withdrawn and centrifuged to measure the absorbance of AM solution at λ_{max} of 521 nm by using a UV-vis spectrophotometer (UH 5300, Hitachi). To determine the dye concentration, calibration plots based on Beer-Lambert's law were established by relating the absorbance to the concentration. The dye degradation efficiency (DE) is calculated from the equation (1) [10]:

$$\mathrm{DE}\,(\%) = \left(\frac{C_0 - C}{C_0}\right) \times 100, \tag{1}$$

where C_0 and C are the AM concentrations at equilibrium and after irradiation (mg l^{-1}), respectively. Control experiments in the absence of a catalyst were carried out with continuous stirring for 6 h. AM is found to be stable upon visible and UVA irradiation resulting in photolysis of less than 5%.

In order to find out the reactive species responsible for the degradation of AM, a series of quenchers were used to scavenge the reactive species. Different amount of quenchers were introduced into the AM solution before catalyst addition. KI (0.1 g l^{-1}), $(CH_3)_2CHOH$ (1 g l^{-1}), NaN_3 (0.01 g l^{-1}), $Cl(CH_2)_2OH$ (0.36 g l^{-1}) and $C_6H_4O_2$ (0.02 g l^{-1}) were used to quench h^+, $^{\bullet}OH$, $^1O_2$, e^- and $^{\bullet}O_2^-$, respectively [10]. In the presence of quenchers, the degradation of AM is suppressed to a certain extent and the decreased apparent first order rate constant (k_{app}) is observed. The k_{app} is determined based on the apparent pseudo-first-order kinetic model according to equation (2):

$$\ln\left(\frac{C_0}{C}\right) = k_{app}t \tag{2}$$

The more the k_{app} is decreased, the more vital the role of the reactive species. The role of the reactive species was indicated by R (%), according to equation (3):

$$R\,(\%) = \left(\frac{k_{app} - k'_{app}}{k_{app}}\right) \times 100, \tag{3}$$

where k'_{app} is the k_{app} in the presence of quencher.

To study the effect of operating parameters on the AM degradation by N-WO_3, the experiments were performed by

Table 1. Properties of the prepared catalysts.

	WO_3	N-WO_3
Crystalline phase	Monoclinic	Monoclinic
Crystalline size (nm)[a]	37.4	17.1
Band gap (eV)[b]	2.66	2.58
XPS peak of N (eV)	Not detected	397.6 (W–N), 400 (N–N; N–O)
XANES peak of N (eV)	Not detected	400.6 ($1s \rightarrow \pi^*$ transitions) 408 ($1s \rightarrow \sigma^*$ transitions)
Specific surface area ($m^2\ g^{-1}$)[c]	10.7	14.3
Average pore diameter (nm)[d]	1.64	10.65
Pore volume ($cm^3\ g^{-1}$)[d]	0.113	0.110
pH_{zpc}	1.9	2.1

[a]Calculated from Scherrer equation.
[b]Calculated by Tauc's method.
[c]Determined based on the Brunauer–Emmett–Teller isotherm.
[d]Calculated from the Barrett–Joyner–Halenda isotherm.

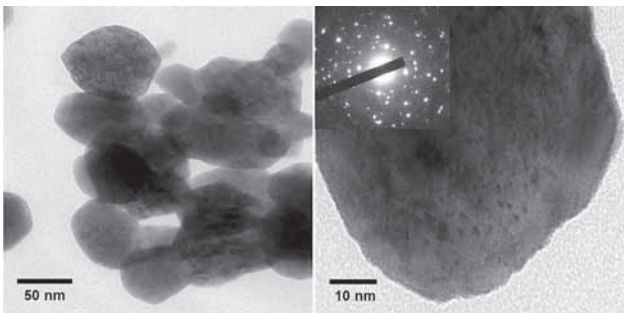

Figure 1. TEM images of N-WO_3 with electron diffraction pattern.

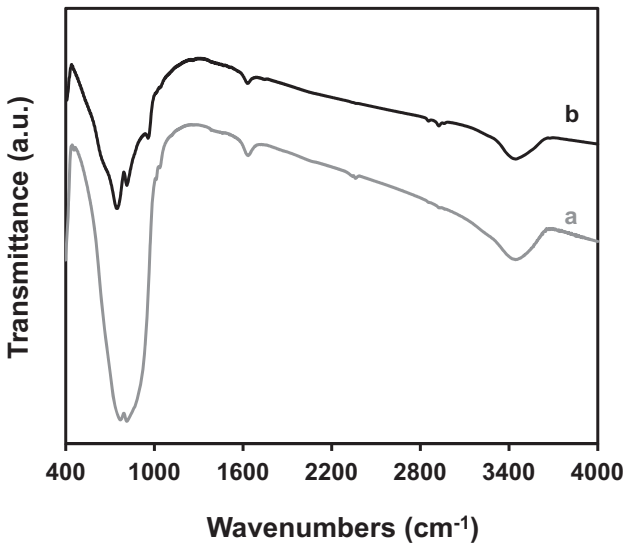

Figure 2. FTIR spectra of (**a**) WO_3 and (**b**) N-WO_3.

varying key operating parameters, namely, dye concentration ($5-25\ mg\ l^{-1}$), catalyst concentration ($0.5-2.5\ g\ l^{-1}$), pH (5–9) and H_2O_2 concentration ($0.1-0.7\ g\ l^{-1}$).

The effects of anions and cations on the photocatalytic degradation of AM by N-WO_3 was investigated by the addition of sodium and sulphate salts, respectively, with a concentration of 0.1 M. Sodium salts were used to avoid the simultaneous effects of cations since Na^+ is at its maximum oxidation state and thus does not compete as a hole scavenger. In addition, Na^+ at concentrations of less than 0.1 M should not affect the charge at the catalyst surface [11]. Sulphate salts were used due to their negligible effect on the photocatalytic activity of N-WO_3.

3. Results and discussion

3.1 *Catalyst properties*

Table 1 summarizes the properties of the catalysts. Compared to WO_3, N-WO_3 has higher specific surface area, lower crystalline size and lower band gap. On the basis of these properties, N-WO_3 is expected to exhibit a higher photocatalytic activity. Furthermore, as shown in figure 1, the diameter of primary particles of N-WO_3 is in the range of 30–70 nm. XPS analysis confirms the presence of W–N bond at 397.6 eV and N–O or N–N bond at 400 eV, while XANES analysis confirms the presence of N_2-like species at 400.6 eV.

The infrared spectra of the catalysts are shown in figure 2. The peaks at around $3440\ cm^{-1}$ are assigned to the O–H stretching modes of adsorbed water and the peak around $1630\ cm^{-1}$ is assigned to the O–H bending of the adsorbed water [12]. The peak centred at $956\ cm^{-1}$ in the WO_3 spectrum is probably due to the vibrations of adsorbed water. Moreover, the strong, broad peak in the fingerprint region of $500-900\ cm^{-1}$ is assigned to the W–O stretching modes [12]. As can be seen, the W–O stretching modes are less intense

for N-WO_3 and the peak is also slightly shifted to a lower wavenumber. This can be an indication of lattice structure alteration after doping with N.

3.2 *Adsorption of AM*

Adsorption of AM on the catalyst is conducted in the absence of light at room temperature. As can be seen in table 2, less than 6% of AM is adsorbed within 1 h under dark condition. Although the difference of the specific surface area between WO_3 and N-WO_3 is not significant, the ability of N-WO_3 to adsorb AM is two times higher than that of WO_3. This is likely due to much higher availability of surface functional groups in N-WO_3. Indeed, the specific surface area usually plays a vital role on the adsorption extent. However, the availability of functional groups on the catalyst surface is also an important factor and determines the adsorption ability of the catalyst.

3.3 *Comparative photocatalytic degradation of AM*

The comparative degradation of AM over time by WO_3, N-WO_3, c/WO_3 and c/N-WO_3 is summarized in table 2. The photocatalytic activity of WO_3 is found to be higher than that of c/WO_3. This may be attributed to the difference in the band gap energy, the availability of surface functional groups and the specific surface area. The doped catalysts show better photocatalytic activity than the pristine counterpart. Moreover, c/N-WO_3 exhibits lower photocatalytic activity than N-WO_3. This is presumably due to ineffective incorporation of N in the WO_3 lattice. In c/N-WO_3, the N dopants may only reside on the surface instead of in the bulk of the catalyst particles. Furthermore, DE under visible light is comparable to that under UVA light because under visible light AM can also be self-degraded after transferring its electron to the CB of the catalyst [13]. In addition, the irradiance of visible light used is much higher than that of the UVA light.

3.4 *Effect of operating parameters on the degradation of AM*

3.4a *Effect of dye concentration*: As can be seen in table 3, with increasing initial AM concentration from 5 to 25 mg l^{-1}, DE decreases from 100 to 86.2% and from 100 to 89.5% for AM degradation under visible and UVA light, respectively. With an increase in initial AM concentration, AM in the bulk of the suspension strongly absorbs incoming light. This leads to reduced light absorption by the catalyst and the generation of electron–hole pairs is then reduced.

3.4b *Effect of catalyst concentration*: For the photocatalytic degradation of 10 mg l^{-1} of AM under visible light, with an increase in catalyst concentration from 0.5 to 1 g l^{-1}, DE increases from 93.5 to 100%. With further increase of catalyst concentration to 2.5 g l^{-1}, DE then decreases to 81.5%. The same pattern is also observed for the photocatalytic degradation of AM under UVA light and the optimum catalyst concentration is found to be 1 g l^{-1}. This can be explained on the basis of two factors, the availability of active sites on the catalyst surface and the light penetration into the suspension system [14]. With an increase in catalyst concentration, the total active surface area increases and the suspension turbidity increases as well. As a result, the light scattering increases leading to decreased light penetration.

3.4c *Effect of pH*: pH of the suspension system is considered to be a critical operating parameter in the photocatalytic degradation of organic compounds. It determines the surface charge of the catalyst particles, the size of formed aggregates, the charge of organic pollutants, the adsorption of organic pollutants onto the catalyst surface and the concentration of $^{\bullet}OH$ radicals generated [15]. As seen in table 3, for the photocatalytic degradation of 10 mg l^{-1} of AM under visible light, DE is observed to be the same (100%) with increasing pH from 5 to 7. Further increase of pH from 7 to 9 decreases DE from 100 to 87.3%. Similarly for the degradation of AM under UVA light, with an increase of pH from 5 to 7, DE is in the same value of 100% and then decreases to 90.1% with further increase of pH to 9. This can be explained as follows. The zero point charge pH of the catalyst is 2.1 (table 1). Therefore, the N-WO_3 surface is negatively charged above pH of 2.1. AM, as an anionic dye, is poorly adsorbed on the surface of N-WO_3 due to electrostatic repulsion by the negatively charged surface of the catalyst. With increasing pH, this electrostatic repulsion is more significant and the adsorption of AM becomes less favourable. As a result, DE is greatly decreased.

Table 2. Efficiency of the catalysts for AM degradation.

Catalyst	Adsorption (%)	DE (%)	
		Vis	UVA
WO_3	2.7 (0.12)	17.1 (0.28)	21.0 (0.48)
c/WO_3	2.1 (0.09)	9.3 (0.24)	10.2 (1.24)
N-WO_3	5.5 (0.29)	100 (0)	100 (0)
c/N-WO_3	3.5 (0.18)	28.3 (3.42)	23.5 (0.36)

Conditions: catalyst concentration (W) = 1 g l^{-1}, AM concentration (C_0) = 5 mg l^{-1}, pH = 7, time (t) = 1 h.
Standard error is in parentheses.

Table 3. Dye degradation efficiency at different operating parameters.

Parameter	Value	DE (%) Vis	DE (%) UVA	Fixed parameter
Dye concentration (mg l^{-1})	5	100 (0)	100 (0)	$W = 1\,g\,l^{-1}$, pH = 7, $t = 1\,h$
	10	100 (0)	100 (0)	
	15	94.5 (1.93)	96.6 (0.16)	
	20	90.2 (0.91)	92.1 (1.72)	
	25	86.2 (4.39)	89.5 (3.37)	
Catalyst concentration (g l^{-1})	0.5	93.5 (0.09)	95.1 (1.82)	$C_0 = 10\,mg\,l^{-1}$, pH = 7, $t = 1\,h$
	1	100 (0)	100 (0)	
	1.5	95.0 (2.1)	96.7 (1.47)	
	2	90.9 (0.29)	88.3 (0.32)	
	2.5	81.5 (0.11)	82.0 (0.61)	
pH	5	100 (0)	100 (0)	$W = 1\,g\,l^{-1}$, $C_0 = 10\,mg\,l^{-1}$, $t = 1\,h$
	6	100 (0)	100 (0)	
	7	100 (0)	100 (0)	
	8	93.2 (0.02)	95.4 (0.45)	
	9	87.3 (1.75)	90.1 (0.66)	
H_2O_2 concentration (g l^{-1})	0	86.2 (4.39)	89.5 (3.37)	$W = 1\,g\,l^{-1}$, $C_0 = 25\,mg\,l^{-1}$, pH = 7, $t = 1\,h$
	0.1	90.1 (3.53)	92.6 (2.36)	
	0.3	98.4 (0.43)	97.3 (0.67)	
	0.5	100 (0)	98.1 (0.62)	
	0.7	96.2 (2.6)	100 (0)	

Standard error is in parentheses.

3.4d *Effect of H_2O_2 concentration*: Hydrogen peroxide is known to beneficially affect the photocatalytic degradation of organic compounds due to the generation of $^{\bullet}OH$ radicals upon photolysis of H_2O_2 by UV light and the inhibition of electron–hole recombination due to its role as an irreversible electron acceptor [15]. However, it was also reported that an excess of H_2O_2 leads to competitive reactions that can inhibit the photocatalytic degradation process [16]. The holes generated by the catalyst may also be consumed by H_2O_2. A similar effect is observed in the degradation of AM by N-WO_3 under visible light. With increasing H_2O_2 concentration, DE increases up to an optimum value (0.5 g l^{-1}) and subsequently decreases. On the contrary, under UVA light, with increasing H_2O_2 concentration to 0.7 g l^{-1}, DE keeps increasing. This may be because H_2O_2 undergoes photolysis producing two additional $^{\bullet}OH$ radicals, which can degrade the dye [17]. The effect of H_2O_2 on the AM degradation is found to depend on the type of light source used.

3.4e *Effect of inorganic ions*: The inhibitory effects of inorganic ions can be attributed to light screening, competitive adsorption to surface active sites, competition for photons, surface deposition of precipitates and elemental metals, radical and hole scavenging and direct reaction with the photocatalyst [18].

The inhibition orders of AM degradation by inorganic ions are determined based on the k_{app} values, shown in table 4 and figure 3. The inhibition of AM degradation by inorganic anions under visible light is in the following order: $CO_3^{2-} > Cl^- > SO_4^{2-} > NO_3^-$. CO_3^{2-} inhibits the degradation of AM quite significantly. The first reason may be due to the weakening of AM adsorption on the catalyst surface. After adding CO_3^{2-}, the catalyst surface becomes more negative due to increased suspension pH. As a result, AM as an anionic species is repelled by the negatively charged surface of N-WO_3. The second reason is probably due to the scavenging character of CO_3^{2-} on the $^{\bullet}OH$ radical as shown in equation (4) [19]:

$$CO_3^{2-} + {}^{\bullet}OH \rightarrow OH^- + {}^{\bullet}CO_3^- \quad (4)$$

Table 4. The k_{app} in the presence of inorganic ions.

Inorganic ions	k_{app} Vis (min^{-1})	k_{app} UVA (min^{-1})
No ion	0.0339 (0.0005)	0.0381 (0.0001)
Cl^-	0.0290 (0.0013)	0.0246 (0.0009)
NO_3^-	0.0319 (0.0005)	0.0283 (0.0007)
CO_3^{2-}	0.0251 (0.0001)	0.0233 (0.0008)
SO_4^{2-}	0.0311 (0.0005)	0.0347 (0.0002)
NH_4^+	0.0335 (0.0001)	0.0372 (0.0009)
Ca^{2+}	0.0252 (0.0001)	0.0218 (0.0003)

Conditions: $W = 1\,g\,l^{-1}$, $C_0 = 25\,mg\,l^{-1}$, pH = 7, ion concentration = 0.1 M.
Standard error is in parenthesis.

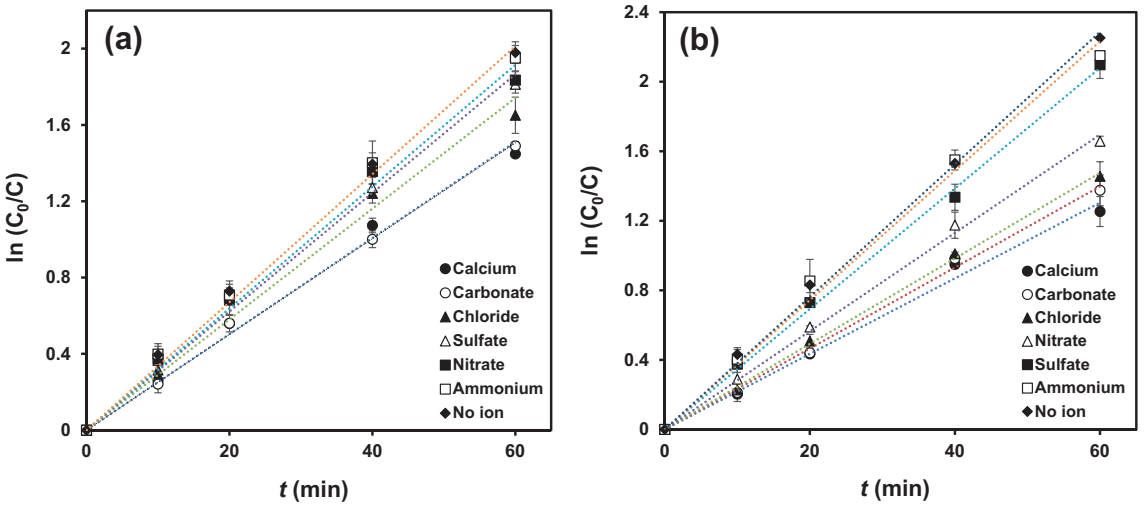

Figure 3. The kinetic plots for pseudo first-order reaction of AM degradation by N-WO_3 **(a)** under visible and **(b)** UVA light in the presence of inorganic ions ($W = 1$ g l^{-1}, $C_0 = 25$ mg l^{-1}, pH = 7, ion concentration = 0.1 M). Error bars denote standard deviation.

One can see that the inhibitory effect of Cl^- is lower than that of CO_3^{2-}. The inhibition by Cl^- can be due to the preferential adsorption displacement over the surface bound OH^- ions [20], which then reduces the generation of $^{\bullet}OH$ radicals. The scavenging of the holes and $^{\bullet}OH$ radicals (equations (5) and (6)) by Cl^- may also inhibit the AM degradation [18]:

$$Cl^- + h^+ \rightarrow {}^{\bullet}Cl \quad (5)$$

$$Cl^- + {}^{\bullet}OH \rightarrow {}^{\bullet}Cl + OH^- \quad (6)$$

Furthermore, the inhibitory effect of SO_4^{2-} is found to be lower than that of Cl^-. Although SO_4^{2-} may also scavenge the holes and $^{\bullet}OH$ radicals (equations (7) and (8)), it is greatly repelled by negatively charged N-WO_3 surface via electrostatic repulsion. Thus, there is no significant inhibition on the adsorption of AM.

$$SO_4^{2-} + h^+ \rightarrow {}^{\bullet}SO_4^- \quad (7)$$

$$SO_4^{2-} + {}^{\bullet}OH \rightarrow {}^{\bullet}SO_4^- + OH^- \quad (8)$$

As for NO_3^-, it may compete for surface active sites that are involved in displacement over the surface bound OH^- ions. However, it can be photolysed forming $^{\bullet}OH$ radicals (equations (9), (10) and (11)) [21]. Therefore, the net result is a negligible inhibitory effect.

$$NO_3^- + h\nu \rightarrow [NO_3^-]^* \quad (9)$$

$$[NO_3^-]^* \rightarrow {}^{\bullet}NO_2 + {}^{\bullet}O^- \quad (10)$$

$$^{\bullet}O^- + H_2O \rightarrow {}^{\bullet}OH + OH^- \quad (11)$$

Under UVA light, the order of photocatalytic inhibition by the anions investigated is $CO_3^{2-} > Cl^- > NO_3^- > SO_4^{2-}$. The inhibition order under UVA light is found to be slightly different than that under visible light. This is due to the difference in the AM degradation mechanism. As seen, the inhibitory effect of NO_3^- is found to be higher than that of SO_4^{2-}. This may be due to the UV screening effect by NO_3^- that inhibits the absorption of photons by the catalyst [22]. One can also see that the reduction of k_{app} is more pronounced in the case of AM degradation under UVA light. This may be because under UVA light $^{\bullet}OH$ is the dominant reactive species. Thus, the reaction of those inorganic ions with $^{\bullet}OH$ results is significantly reduced k_{app}.

Under both visible and UVA light, the inhibitory effect of NH_4^+ is lower than that of Ca^{2+}. NH_4^+ shows negligible effects since it is at its maximum oxidation state and thus is incapable of inhibiting the photocatalytic process. Although Ca^{2+} as well is at its maximum oxidation state, it may be reduced by the photogenerated electron and deposited on the catalyst surface. The deposition of Ca^0 hinders the adsorption of AM. Additionally, the compression of the electrical double layer at a high Ca^{2+} concentration of 0.1 M may induce catalyst aggregation and precipitation [23].

Overall, inorganic ions, such as CO_3^{2-}, Cl^- and Ca^{2+}, which are ubiquitous components in textile effluents are found to negatively affect the photocatalytic performance of N-WO_3 in degrading AM. Hence, to achieve high degradation efficiency the concentration of such ions should be strictly controlled, especially Ca^{2+} and CO_3^{2-}. The concentration of those ions should be less than 0.1 M.

3.5 *Mechanism of AM degradation by N-WO_3*

In the case of N-WO_3, the excitation of electrons upon irradiation takes place through different pathways: (1) electrons are excited from VB to CB via an energy level formed by oxygen

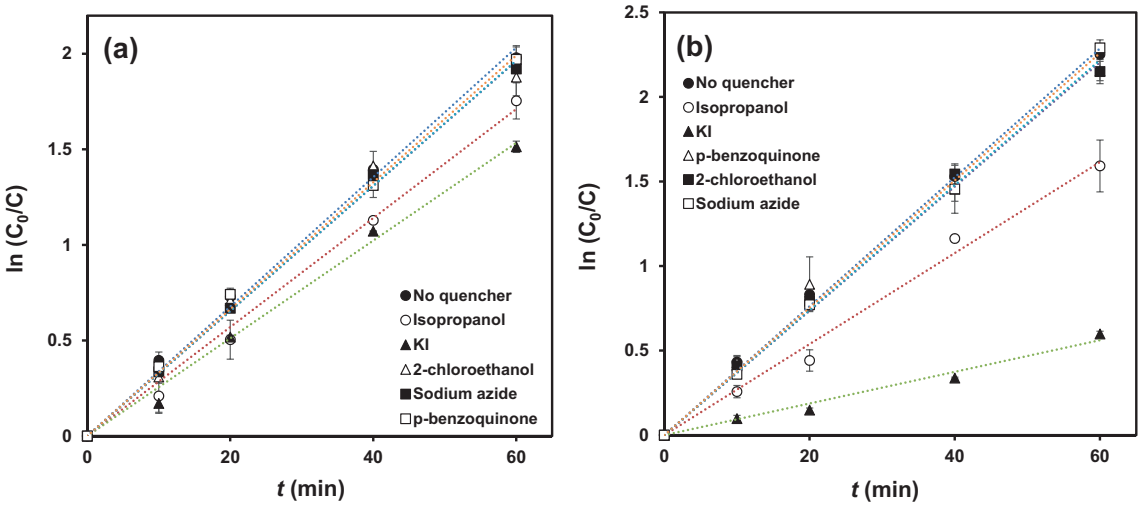

Figure 4. The kinetic plots for pseudo first-order reaction of AM degradation by N-WO_3 **(a)** under visible and **(b)** UVA light in the presence of quenchers ($W = 1\ g\ l^{-1}$, $C_0 = 25\ mg\ l^{-1}$, pH = 7). Error bars denote standard deviation.

Table 5. The k_{app} in the presence of quenchers.

Quencher	Quenched reactive species	Vis/N-WO_3		UVA/N-WO_3	
		k_{app} (min^{-1})	R (%)	k_{app} (min^{-1})	R (%)
No quencher	—	0.0339 (0.0005)	—	0.0381 (0.0001)	—
KI	h^+	0.0256 (0.0003)	24.4 (2.30)	0.0094 (0.0002)	75.2 (0.78)
Isopropanol	$^{\bullet}OH$	0.0285 (0.0012)	15.8 (5.15)	0.0269 (0.0012)	29.6 (5.63)
NaN_3	$^1O_2$	0.0328 (0.0001)	3.3 (1.82)	0.0376 (0.0001)	1.3 (0.01)
2-Chloroethanol	e^-	0.0327 (0.0004)	3.5 (2.86)	0.0369 (0.0009)	2.9 (1.48)
p-Benzoquinone	$^{\bullet}O_2^-$	0.0332 (0.0004)	2.1 (0.38)	0.0367 (0.0010)	3.4 (2.95)

Conditions: $W = 1\ g\ l^{-1}$, $C_0 = 25\ mg\ l^{-1}$, pH = 7.
Standard error is in parentheses.
The role of reactive species is in the following order:
Vis/N-WO_3 : $h^+ > {}^{\bullet}OH > e^- > {}^1O_2 > {}^{\bullet}O_2^-$.
UVA/N-WO_3 : $h^+ > {}^{\bullet}OH > {}^{\bullet}O_2^- > e^- > {}^1O_2$.

vacancy (O_v); (2) electrons are directly excited from VB to CB; (3) electrons are excited from VB to CB via a mid-band state of 2p orbitals of N (N_{2p}); (4) electrons are excited from N_{2p} to CB.

Upon visible light irradiation, the electrons in AM are excited and can be transferred to the CB of N-WO_3. This photosensitization mechanism involves electron transfer from the AM to the N-WO_3. After light absorption by the adsorbed AM, an electron in AM is excited from the highest occupied molecular orbital (HOMO) to the lowest unoccupied molecular orbital (LUMO). This excited electron can be transferred to the CB of N-WO_3. This process is thermodynamically favourable due to the low CB potential of N-WO_3. The CB of WO_3 is +0.3 V *vs*. NHE at pH 7 [9].

It should be noted that the photocatalytic activity of N-WO_3 under visible light can also be due to the direct oxidation of AM by h^+ generated either in the mid-band gap state or in the VB. However, direct reduction of AM by e^- is not likely to occur due to the lower CB potential of N-WO_3 as compared to the LUMO potential of AM. Moreover, due to the same reason of low CB potential in the case of pristine WO_3, e^- accumulated in the CB cannot be consumed by the electron acceptors available in the system, such as O_2 and AM, and thus quickly recombines with h^+ in the VB. This results in low quantum efficiency. However, for N-WO_3, e^- does not recombine with h^+ because it is trapped by N dopants, which acts as e^- traps. As a result, the photocatalytic activity is greatly enhanced.

3.6 *Role of reactive species*

Photocatalytic activity of a catalyst depends not only on light absorption ability, but also on types of reactive species produced. This is because reactive species have different oxidation and reduction powers. To elucidate the role of reactive species during the degradation of AM, chemical quenching techniques were employed [10].

As seen in figure 4, the AM degradation by N-WO_3 in the presence of quenchers under visible and UVA light follows a pseudo first-order kinetic model. Table 5 shows the k_{app}, with or without the presence of the quenchers. With the addition of quenchers, the k_{app} is found to decrease. Under both visible and UVA light, a significant role of h^+ is observed. This is because upon irradiation, h^+ is generated not only in the VB, but also in the mid-gap state formed by the N dopant (N_{2p}). The h^+ participates in the photocatalytic degradation process by directly attacking AM on the catalyst surface. Small reductions of k_{app} with the addition of $(CH_3)_2CHOH$ suggest that $^{\bullet}OH$ contributes to the degradation of AM to a lesser extent. Negligible inhibition of k_{app} with the addition of NaN_3, *p*-benzoquinone and $Cl(CH_2)_2OH$ suggests that $^1O_2$, $^{\bullet}O_2^-$ and e^- have a very minor role in the AM degradation. The minor roles of $^1O_2$ and $^{\bullet}O_2^-$ are due to the lower CB edge of N-WO_3. As a result, the one-electron reduction process, which generates $^{\bullet}O_2^-$ from the reaction between O_2 and e^- cannot occur. Due to unavailability of $^{\bullet}O_2^-$, h^+ cannot react with $^{\bullet}O_2^-$ to produce $^1O_2$.

It is important to note that the role of h^+ under visible light is less significant than that under UVA light. This indicates that dye sensitization mechanism is the major pathway for the degradation of AM under visible light instead of dye oxidation by reactive radicals. The existence of dye sensitization as the major pathway is supported by the fact that this sensitization process is thermodynamically highly favourable. During the sensitization process, an excited electron from the LUMO of AM can be easily transferred to the CB of N-WO_3 due to considerably low CB potential of N-WO_3. In contrast, oxidation of AM by reactive radicals is the main pathway for AM degradation under UVA light as dye sensitization cannot occur under UV light.

Conclusions

N-doped WO_3 photocatalyst is successfully synthesized by thermal decomposition of peroxotungstic acid–urea complex and is evaluated for the degradation of toxic dye AM. N doping into WO_3 greatly enhances the photocatalytic activity for the AM degradation. The quenching experiment shows the negligible role of $^{\bullet}O_2^-$ in the AM degradation under visible and UVA light. This indicates the absence of the one-electron transfer mechanism due to the unsuitability of the CB potential for O_2 reduction. h^+ plays a key role in the degradation of AM under visible and UVA light, while $^{\bullet}OH$ contributes to a lesser extent. The dye sensitization mechanism is the main pathway for the degradation of AM under visible light. This is due to the considerably low CB potential of N-WO_3 allowing efficient electron transfer from AM to the CB. Under UVA light, AM is degraded mainly through oxidation by h^+. This is due to the very deep VB potential of N-WO_3, capable of generating h^+ with strong oxidation power. Using 1 g l^{-1} of N-WO_3, 10 mg l^{-1} of AM can be degraded with 100% efficiency within 1 h at pH 7 under both visible and UVA light. Moreover, CO_3^{2-}, Cl^-, NO_3^-, SO_4^{2-} and Ca^{2+} are found to inhibit the degradation of AM, while NH_4^+ shows negligible influence.

Acknowledgements

This work is supported by the Sirindhorn International Institute of Technology through an Excellent Foreign Student (EFS) doctoral scholarship.

References

[1] Xin G, Guo W and Ma T 2009 *Appl. Surf. Sci.* **256** 165
[2] Bamwenda G R and Arakawa H 2001 *Appl. Catal. A: Gen.* **210** 181
[3] Morales W, Cason M, Aina O, de Tacconi N R and Rajeshwar K 2008 *J. Am. Chem. Soc.* **130** 6318
[4] Miyauchi M 2008 *Phys. Chem. Chem. Phys.* **10** 6258
[5] Bamwenda G R, Sayama K and Arakawa H 1999 *J. Photochem. Photobiol. A: Chem.* **122** 175
[6] Abe R, Takami H, Murakami N and Ohtani B 2008 *J. Am. Chem. Soc.* **130** 7780
[7] Arai T, Horiguchi M, Yanagida M, Gunji T, Sugihara H and Sayama K 2008 *Chem. Commun.* 5565 https://doi.org/10.1039/B811657A
[8] Arai T, Horiguchi M, Yanagida M, Gunji T, Sugihara H and Sayama K 2009 *J. Phys. Chem. C* **113** 6602
[9] Kim J, Lee C W and Choi W 2010 *Environ. Sci. Technol.* **44** 6849
[10] Antonopoulou M, Giannakas A, Deligiannakis Y and Konstantinou I 2013 *Chem. Eng. J.* **231** 314
[11] Wang D, Li Y, Puma G L, Wang C, Wang P, Zhang W *et al* 2015 *J. Hazardous Mater.* **285** 277
[12] Nogueira H I, Cavaleiro A M, Rocha J, Trindade T and de Jesus J D P 2004 *Mater. Res. Bull.* **39** 683
[13] Banerjee S, Pillai S C, Falaras P, O'shea K E, Byrne J A and Dionysiou D D 2014 *J. Phys. Chem. Lett.* **5** 2543
[14] Daneshvar N, Salari D and Khataee A 2004 *J. Photochem. Photobiol. A: Chem.* **162** 317
[15] Sun J, Qiao L, Sun S and Wang G 2008 *J. Hazardous Mater.* **155** 312
[16] Daneshvar N, Salari D and Khataee A 2003 *J. Photochem. Photobiol. A: Chem.* **157** 111
[17] Stefan M I, Hoy A R and Bolton J R 1996 *Environ. Sci. Technol.* **30** 2382
[18] Chong M N, Jin B, Chow C W and Saint C 2010 *Water Res.* **44** 2997
[19] Guillard C, Lachheb H, Houas A, Ksibi M, Elaloui E and Herrmann J-M 2003 *J. Photochem. Photobiol. A: Chem.* **158** 27
[20] Wang D, Li Y, Li G, Wang C, Zhang W and Wang Q 2013 *J. Hazardous Mater.* **254** 64
[21] Zhang X, Wang Y and Li G 2005 *J. Mol. Catal. A: Chem.* **237** 199
[22] Burns R A, Crittenden J C, Hand D W, Selzer V H, Sutter L L and Salman S R 1999 *J. Environ. Eng.* **125** 77
[23] Thio B J R, Montes M O, Mahmoud M A, Lee D-W, Zhou D and Keller A A 2011 *Environ. Sci. Technol.* **46** 6985